Structure
Article

Transient Domain Interactions Enhance the Affinity of the Mitotic Regulator Pin1 toward Phosphorylated Peptide Ligands

Anja Matena,[1,7] Christian Sinnen,[3,7] Johannes van den Boom,[1] Christoph Wilms,[2] J. Nikolaj Dybowski,[4] Ricarda Maltaner,[1] Jonathan W. Mueller,[1,5] Nina M. Link,[1,6] Daniel Hoffmann,[2] and Peter Bayer[1,*]
[1]Research Group Structural and Medicinal Biochemistry
[2]Research Group Bioinformatics
ZMB, University of Duisburg-Essen, 45117 Essen, Germany
[3]Solupharm Pharmazeutische Erzeugnisse GmbH, Industriestraße 3, 34212 Melsungen, Germany
[4]Evotec (Munich) GmbH, Am Klopferspitz 19a, 82152 Martinsried, Germany
[5]Centre for Endocrinology, Diabetes, and Metabolism (CEDAM), School of Clinical and Experimental Medicine, University of Birmingham, Institute of Biomedical Research, Wolfson Drive, Birmingham B15 2TT, UK
[6]Research Group Computational and Systems Biology, Biozentrum, University of Basel, Klingelbergstrasse 50/70, CH-4056 Basel, Switzerland
[7]These authors contributed equally to this work
*Correspondence: peter.bayer@uni-due.de
http://dx.doi.org/10.1016/j.str.2013.07.016

SUMMARY

The mitotic regulator Pin1 plays an important role in protein quality control and age-related medical conditions such as Alzheimer disease and Parkinson disease. Although its cellular role has been thoroughly investigated during the past decade, the molecular mechanisms underlying its function remain elusive. We provide evidence for interactions between the two domains of Pin1. Several residues displayed unequivocal peak splits in nuclear magnetic resonance spectra, indicative of two different conformational states in equilibrium. Pareto analysis of paramagnetic relaxation enhancement data demonstrates that the two domains approach each other upon addition of a nonpeptidic ligand. Titration experiments with phosphorylated peptides monitored by fluorescence anisotropy and chemical shift perturbation indicate that domain interactions increase Pin1's affinity toward peptide ligands. We propose this interplay of the domains and ligands to be a general mechanism for a large class of two-domain proteins.

INTRODUCTION

Kinases involved in cell cycle and downstream signaling, such as cyclin-dependent kinases and MAP kinases, target serine/threonine-proline motifs in various proteins. The phosphorylation of such motifs is usually followed by *cis/trans* isomerization of the Xaa-Pro peptide bond as a prerequisite for proper function and, ultimately, proper dephosphorylation. Hence, this isomerization constitutes an important molecular switch by which cell cycle events and protein-folding processes are triggered (Liou et al., 2011). In humans, there is only one central enzyme to fulfill this task, the mitotic regulator Pin1 (Lu et al., 1996), which has been implicated in several severe diseases, including different types of cancer as well as Alzheimer disease and Parkinson disease (Yeh and Means, 2007). Consequently, there is a strong interest in this enzyme, both for basic research and for the pharmaceutical industry, reflected by a plethora of publications and an increasing number of patents on Pin1 inhibitors (Bayer et al., 2005; Duncan et al., 2011; Guo et al., 2009; Liu et al., 2010, 2012; Xu et al., 2012).

As a catalytic domain, Pin1 contains a phosphorylation-specific peptidyl-prolyl *cis/trans* isomerase (PPIase) domain of the parvulin type (Ranganathan et al., 1997; Mueller and Bayer, 2008) that harbors a highly conserved network of hydrogen bonds (Mueller et al., 2011). This domain has the typical folding topology of all parvulins (Sekerina et al., 2000; Kühlewein et al., 2004; Li et al., 2005; Jaremko et al., 2011). The PPIase domain is N-terminally flanked by a WW domain that can also bind Ser/Thr (P)-Pro motifs (Verdecia et al., 2000). The two domains are connected by a flexible linker (Bayer et al., 2003). Crystal structures indicate close contact between the two domains (Ranganathan et al., 1997; Verdecia et al., 2000; Zhang et al., 2007). This tight domain arrangement is in stark contrast to nuclear magnetic resonance (NMR) studies of Pin1 (Jacobs et al., 2003; Bayer et al., 2003), where no interdomain NOEs could be detected for the apo-enzyme in solution.

Lu and Zhou postulated a "tag-and-twist" mechanism for Pin1 function (Lu and Zhou, 2007) in which the WW domain targets Pin1 specifically to doubly or multiply phosphorylated substrates that are subsequently isomerized by the PPIase domain. According to this hypothesis, isomerization rates should increase from singly to doubly phosphorylated substrates; however, the opposite tendency was described for multiphosphorylated tau peptides (Smet et al., 2005; Innes et al., 2013). Remarkably, the isolated PPIase domain displays an approximate 4.5-fold higher isomerase activity than the full-length Pin1 enzyme (Peng et al., 2009). This already indicates that the interaction between the catalytic domain and the WW domain

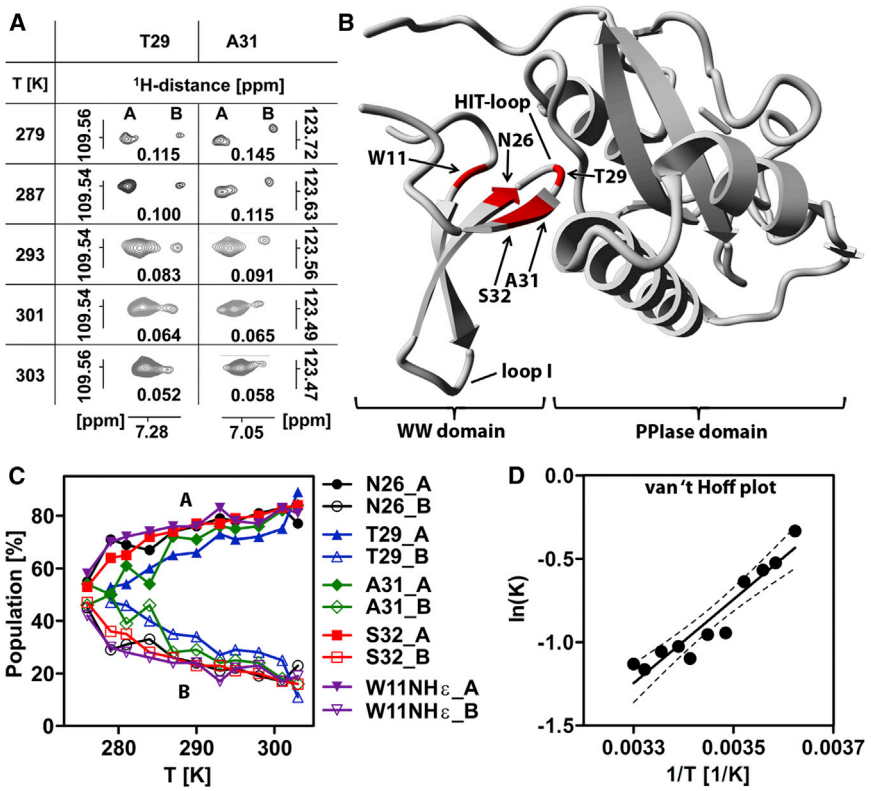

Figure 1. Peak Splits Detected in HSQC Spectra of Pin1

(A) Sections of ^{1}H-^{15}N-HSQC spectra at various temperatures showing the split HN resonances of T29 and A31 within the WW domain. The respective ^{1}H distances in ppm are denoted below. Split resonances are indicated with A and B, respectively.

(B) Mapping of residues W11NHε, N26, T29, A31, and S32 (red) on the closed Pin1 structure (Protein Data Bank [PDB] 1PIN). The resonances of all these residues display pronounced peak splitting.

(C) The relative populations of the two states A and B change at increasing temperature. Relative mean peak heights are indicative of the equilibrium at each temperature. A plot of these peak heights versus temperature indicates increasing energetic differences with elevated temperatures.

(D) van't Hoff plot for determining thermodynamic parameters of domain interaction. Averaged values from N26, T29, A31, S32, and W11NHε are shown. Dashed lines indicate a 95% confidence interval for the linear regression.

See also Figures S1 and S2.

is complex. The two domains tumble independently, but upon high-affinity substrate binding, they behave like a single entity (Jacobs et al., 2003). Extensive medium- to long-range effects within the WW domain have been revealed by modeling upon ligand binding (Morcos et al., 2010). Complementary, a stiffening of a row of hydrophobic side chains has also been described in the interior of the PPIase domain (Namanja et al., 2007, 2011).

Here, we propose a unifying model, stating that weak interdomain interactions tune the function of Pin1, and we provide supporting evidence with NMR spectroscopy data. Several NMR resonances within spatial proximity to the second loop of the WW domain, loop II, displayed unequivocal peak splitting in heteronuclear single quantum coherence (HSQC) experiments (Figure 1A), indicative of two different chemical states. Because this loop contains the amino acid motif His-Ile-Thr, we from now on refer to it as the HIT-loop. Taking these split resonances as indicators for two conformations in equilibrium, we derived a standard enthalpy in the range of −2 kJ/mol for this domain interaction, too weak to be accessible by calorimetry. As in various crystal structures of Pin1, a PEG moiety is found at the domain interface; we tested whether this nonpeptidic low-molecular-weight compound influences domain interaction. With Pareto analysis of paramagnetic relaxation enhancement, we confirmed a tightening of this weak domain interaction upon the addition of polyethylene glycol (PEG400). The domain interaction also has functional implications; it seemingly increased Pin1's affinity toward peptide ligands. From molecular dynamics simulations, we derived a model in which the back part of the PPIase domain—seen from the catalytic cleft—serves to present the WW domain for optimized ligand binding. Our findings indicate that a molecular binding partner regulates domain interaction and substrate affinity in Pin1 and may not only serve as a paradigm for WW-containing proteins, but may also be extended to multidomain proteins in general (Kovermann et al., 2011).

RESULTS

Split NMR Resonances Indicate Two Conformations of the Pin1 Protein in Solution

Close scrutiny of ^{1}H-^{15}N-HSQC spectra of Pin1 recorded at 285 K, in contrast to 300 K in former NMR measurements, revealed splitting of resonances for HN signals of residues N26, T29, A31, and S32 as well as for W11NHε, all within the second loop of the WW domain, the HIT loop (Figure 1A). This observation has escaped detection in previous NMR studies of Pin1 (Bayer et al., 2003; Jacobs et al., 2003). In a series of ^{1}H-^{15}N-HSQC spectra recorded at temperatures ranging from 276 K to 303 K, split resonances of each peak move toward each other with increasing temperature (Figure 1B). The observed temperature dependence indicates forthcoming coalescence of split resonances at higher temperatures (Figure S1 available online) and implies the existence of two conformations undergoing chemical exchange that we refer to as A and B from now on. The split signals are broadened and exhibit interleaving shapes at 298 K; this indicates that the two conformations are in intermediate exchange with a rate of interconversion in the range of 1–10^3 sec^{-1}. At this temperature, a mean lifetime $\tau = 1/k_{ex}$ for the two states between 11 and 17 ms was calculated from the ^{1}H chemical shift distances of A and B. Lifetimes in the range of milliseconds are predominantly related to domain reorientations or domain interaction processes in proteins (Gardino and Kern,

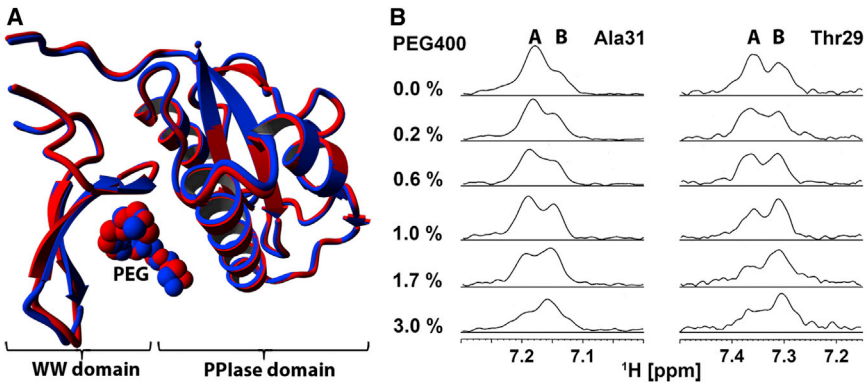

Figure 2. The Interdomain Ligand PEG400 Influences the Equilibrium between the Two Populations

(A) Overlay of Pin1 crystal structures (PDB 1PIN, blue; PDB 2ZQT, red) highlighting part of a bound polyethylene glycol (PEG400) chain.

(B) Orthogonal projections of NH signals. Split resonances onto the ^{1}H axis demonstrate reversion of the population of the two conformations A and B upon addition of increasing amounts of PEG400. NH signals of T29 and A31 are shown from measurements at 300 K.

2007). Substantial reorientation of domains in Pin1 was already observed upon substrate binding (Jacobs et al., 2003). We have previously postulated that domain interaction also occurs in substrate-free Pin1 solutions, and substrate binding was thought to shift the equilibrium between noninteracting (open) and interacting (closed) WW and PPIase domains toward the closed state (Bayer et al., 2003). ^{1}H-^{15}N-HSQC spectra of the isolated WW domain showed no peak splits for any of the resonances mentioned above (Figure S2A). Moreover, peak splits caused by transient interdomain contacts were sensitive to linker shortening (Figure S2B), indicative of a critical role of the linker length for proper domain arrangement. Consequently, it should be possible to assign split resonances A and B of each NH signal to open and closed conformations of Pin1 (Figure 1A).

Thermodynamic Parameters Confirm Transient Interdomain Interaction

The absence of interdomain NOEs (Bayer et al., 2003) and the calculated short lifetime of the intramolecular complex indicate a transient interaction of the domains. We can assume that both conformations exist in equilibrium because the chemical shifts of A and B reflect the contributions from each conformational species weighted by its population. The equilibrium constant K_{eq} = pB/pA for transition A ↔ B can be calculated from signal heights of the split resonances at any measured temperature (Figure 1C). From the temperature dependence of ln (K_{eq}), an enthalpy change for the domain interaction of −2.1 kJ/mol was estimated (Figure 1D), pointing to a slightly favored conformation A under the study conditions.

PEG400 Modulates Relative Population of the Two Conformational States

Various X-ray structures of the full-length Pin1 protein available in the public domain present a model in which both domains interact via a small interface (Ranganathan et al., 1997; Zhang et al., 2007; Verdecia et al., 2000; Guo et al., 2009; Liu et al., 2010, 2012). In these studies, polyethylene glycol (PEG) was used as precipitating additive forcing protein crystallization and/or as a cryopreservative. The interface cavity in all these structures is still occupied by a PEG molecule, putatively tightening domain interaction and favoring a closed conformation (Figure 2A). We previously reported, with ^{1}H-^{15}N-HSQC NMR, that PEG400 induces large chemical shifts of the HN resonance of Q33, a residue at the proposed domain interface of Pin1 (Bayer et al., 2003). Further tests should elucidate the influence of increasing concentrations of PEG400 onto the observed split resonances of N26, T29, A31, S32, and W11NHε of Pin1 by ^{1}H-^{15}N-HSQC spectra. Of note, increasing levels of PEG400 did not induce notable chemical shifts in these resonances (in contrast to shifts in other, more studied residues such as Q33; Bayer et al., 2003). Looking again at the peak heights of conformations A and B, we made the unexpected observation that PEG400 induced an inversion of relative peak heights of pairs of resonances for W11NHε, N26, T29, A31, and S32 in a concentration-dependent manner (Figure 2B). At 3% PEG400, signal intensities of A and B were reversed: resonance B gained in relative height whereas conformation A lost intensity. Precipitation of Pin1 hampered spectra acquisition at even higher concentrations of PEG400. This finding is in agreement with the observation that PEG400 can increase the chemical potential of proteins in solution, thus destabilizing its solution state and enforcing protein amorphization or crystallization (Arakawa and Timasheff, 1985). As conformation B was favored at high PEG400 concentration similar to crystallizing conditions, we interpreted conformation B as a crystal-like state. Most likely, conformation B represents a PEG400-bound closed state exhibiting a domain arrangement similar to the crystal structures of Pin1. Chemical shift data of the two Pin1 domains in the presence and absence of each other revealed that the number of amino acids involved in domain interaction in solution exceeds the number of residues observed at the interface in the crystal structure (Figure S3), indicating that domain interaction is more intricate than a mere open-close equilibrium.

Monitoring the Effect of PEG400 on the Spatial Domain Arrangement by PRE

To experimentally determine the effect of PEG400 on domain interactions, NMR paramagnetic relaxation enhancement (PRE) measurements were performed using a paramagnetic PROXYL label. The unpaired electron of the pyrrolidinyloxy moiety has a strong dipolar moment that interacts with NMR-active nuclei at distances of approximately 20–25 Å (Gillespie and Shortle, 1997; Battiste and Wagner, 2000). Affected moieties show increased relaxation behavior and, consequently, reduced signal intensity in a distance-dependent manner (r^{-6}). This most often allows the extraction of long-range distance information for dynamic systems.

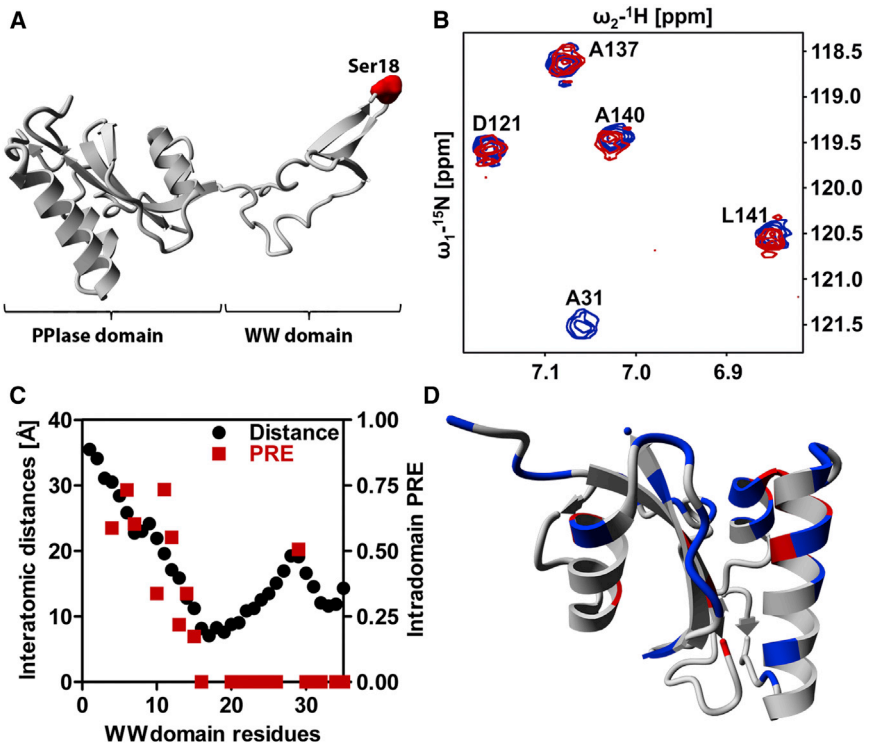

Figure 3. Paramagnetic Relaxation Enhancement Monitors Changes Induced by the Presence of PEG400 at the Interdomain Interface

(A) NMR structure of full-length Pin1 (PDB 1NMV_8) in an open conformation highlighting the prominent position of serine 18 within loop 1 of the WW domain. A S18C mutant served as attachment point for the paramagnetic PROXYL label.

(B) The HN signal of residue A31 is shown in the ^{1}H-^{15}N-HSQC spectrum that vanishes completely upon PROXYL labeling. This is due to an increased T2 relaxation time of the respective nuclei that contribute to this HN signal. Resonances D121, A137, A140, and L141 are also shown; they are not affected by the label.

(C) The paramagnetic relaxation enhancement (PRE) on the HN signals within the WW domain of Pin1 is plotted versus the interatomic distances from the respective amide nitrogen atoms. These distances were calculated relative to the oxygen atom of the actual NO radical within the pyrrolidinyloxy moiety that was modeled onto the structure 1NMV_8.

(D) Mapping of PREs within the PPIase domain of PROXYL-labeled Pin1 with and without the interdomain ligand PEG400. Residues showing PREs in the absence (blue) and additionally in the presence (red) of PEG400 are highlighted on the PPIase domain structure of Pin1 (PDB 1NMW). Only vanishing signals and those exhibiting PRE values < 0.5 are mapped. Small numbers represent large PREs in this case. These data did not allow the direct extraction of distance constraints by classical approaches, probably due to the very high dynamics of the system.

See also Figure S3.

Residue S18 is one of the amino acids most distant from the PPIase domain in the compact crystal structures 1PIN and 2Q5A and resides in the flexible loop I region (Figure 1B) implicated in WW domain-ligand binding (Peng et al., 2009; Jager et al., 2008). Hence, we chose this residue to attach the paramagnetic PROXYL label via covalent coupling in the triple mutant Pin1$_{S18C/C57A/C113A}$ in which the two endogenous cysteines were removed and S18 was changed to cysteine (Figure 3A). Coupling was verified with mass spectrometry. ^{1}H-^{15}N-HSQC spectra of the labeled mutant were recorded and reassigned according to Jacobs and colleagues (Jacobs et al., 2003). PREs were calculated from the signal-to-height ratio I_{ox}/I_{red} of peak intensities extracted from HSQC spectra recorded after (I_{ox}) and before (I_{red}) labeling with PROXYL-iodoacetamide (Table S1). Several signals vanish in the presence of the label due to strong PREs. As an example, the resonance for A31 is shown in the respective section of the ^{1}H-^{15}N-HSQC spectrum (Figure 3B). Extinction of signals was observed for atom-PROXYL distances of up to 22 Å within the WW domain, providing us with a ruler to define the lower and upper limits of the observable PRE (Figure 3C). This effective radius was in very good agreement with the values reported previously (Battiste and Wagner, 2000). In the absence of PEG, we also observed PRE effects within the PPIase domain. It seemed that residues within a negative patch around Glu100 as well as residues starting from Gly144 were already selectively affected by the paramagnetic probe. This may be taken as additional evidence that a minor population of the protein is in the closed conformation even in the absence of ligands. With this molecular probe at hand, we went to determine the influence of PEG400 on PRE signals within the PPIase domain.

PEG400 Strengthens Domain Interaction

Within the PPIase domain, the paramagnetic label induced significantly increased relaxation behavior of several HN resonances in the presence of 2% of PEG400, pointing to a reduced average distance and/or tighter interaction of WW and PPIase domain (Figure 3D). However, the very high motional flexibility of this system made it difficult to transform the PRE data into definite distances as has been done recently for another complex (Madl et al., 2011). Therefore, we set out to explore the space of relative geometric arrangements of PPIase and WW domains in the presence and absence of PEG400 computationally, applying two constraints derived from our PRE experiments (Figure S4). The set of arrangements that were Pareto-optimal with respect to these constraints were considered the best explanation of experimental data. We found that domain distances decreased and domain interaction was tightened in the presence of PEG400 (Figure 4A). To interpret our findings at the molecular level, full-length Pin1 was subjected to 100 ns of all-atom molecular dynamics (MD) simulations both with and without a PEG molecule. During the complete simulation time, the position of Ser18 was monitored relative to various residues within the PPIase domain. In the presence of PEG, all of these distances were constantly shorter than in its absence (Figure 4B). As a control, such MD simulations (100 ns with and without PEG) were repeated for the Arg14Ala mutant that was crystallized in the

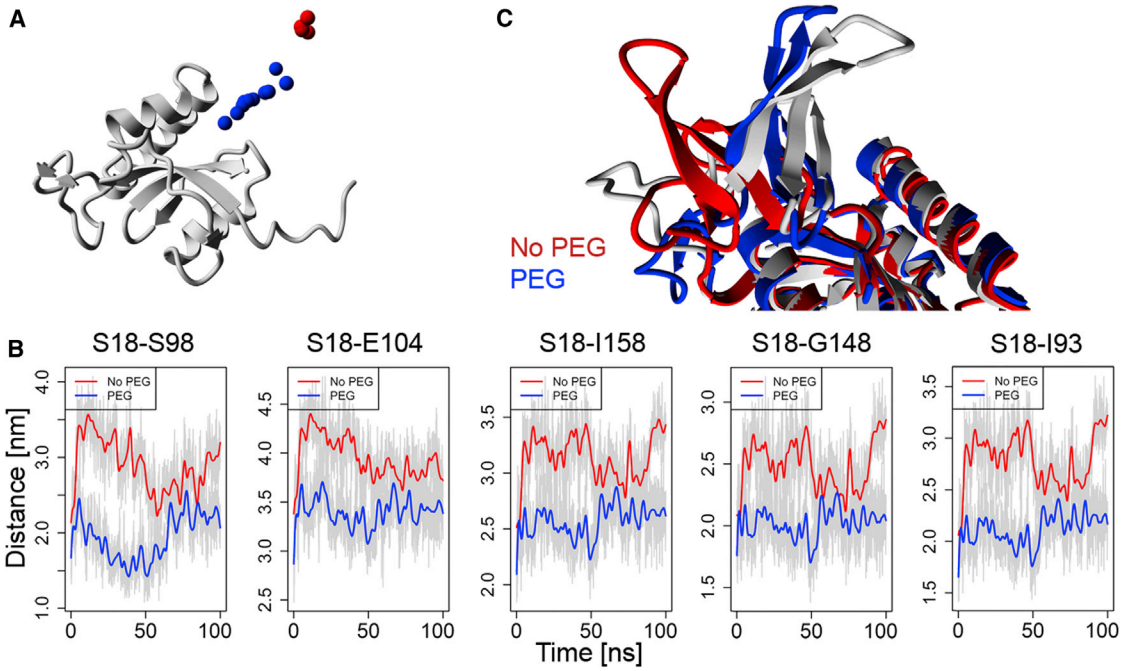

Figure 4. PEG400 Enhances Interdomain Interaction within the Two-Domain Pin1 Protein

(A) Interpretation of the PEG400 titration of PROXYL-labeled Pin1 is a multiparameter problem. Hence, we applied Pareto-optimization to find those positions of the PROXYL label within the WW domain that best represent our data set. These positions are depicted as spheres relative to the PPIase domain (gray) in the presence (red) and absence (blue) of PEG400. Another possible solution is calculated for the absence of PEG at 32 Å from the red sphere cluster was omitted for better visualization.

(B) Traces from 100 ns all-atom MD simulation experiments performed in the presence (blue) and absence (red) of PEG400. A model of Pin1 was built using a crystal structure (PDB 2Q5A) with a modeled linker and subjected to simulations with and without the polyethylene glycol molecule. The atomic distances of the β-carbon atom of S18 to selected residues in the PPIase domain are plotted throughout the whole simulation period.

(C) Overlay of structures from snapshots after 100 ns MD simulation without (red) and with (blue) the polyethylene glycol molecule on the Pin1 crystal structure (gray; PDB 2Q5A).

See also Figure S4.

original study reporting the 2Q5A structure (Zhang et al., 2007), essentially with the same result (data not shown). To depict the results of MD simulations, snapshots after 100 ns simulation time were compared to the initial model (Figure 4C). Except for minor movement of loop I and the adjacent regions of the WW domain, the simulation outcome with PEG resembles the starting structure. In all simulations, the HIT loop remained close to Ala137 within helix 4 and Gly148 of beta-strand 3 of the catalytic domain, while the loop I and the adjacent regions of the WW domain moved away from these residues. In contrast, the simulation without PEG revealed a large movement of the WW domain away from the respective part of the PPIase domain.

Biologic Consequences of Domain Interaction

Finally, we tested whether the ligand-binding properties of Pin1 were influenced by PEG. Therefore, the affinity of Pin1 toward phosphorylated peptide ligands was studied with two complementary approaches. First, the binding of the fluorescently labeled model peptide RhodamineB-GGGApSPF-NH_2 to Pin1 was monitored by adding increasing amounts of protein to the peptide while following its change in fluorescence anisotropy in the presence and absence of 2% PEG400 (Figure 5A). The macromolecular K_D values were extrapolated using the population data from the ^1H-^{15}N-HSQC temperature titration experiments. The K_D values for the open and closed conformations deviate by a factor of two, pointing to different affinities to substrate molecules (Figure 5B). Thereby, the open conformation exhibits a higher K_D value and is binding with less affinity to the peptide substrate.

A similar result was obtained from ^1H-^{15}N-HSQC titration experiments in the presence and absence of 2% PEG400 using the peptide Suc-ApSPF-pNA (Figure 5C). K_D values for peptide binding obtained from chemical shift perturbation of the open (A) and closed (B) conformation deviate by a factor of two (Figure 5D), which is in good agreement with the fluorescence anisotropy data. Because the chemical shifts are derived from resonances of residues within the WW domain, the affinity differences observed in the closed and opened conformation might be correlated with substrate binding to the WW domain.

DISCUSSION

We have used a set of complementary methods to gain a comprehensive picture of the structural variety of the two-domain protein Pin1 in the presence and absence of ligands. In molecular biology, functional ligand binding has generally been recognized as a key process early on and prompted the development of handy models to explain observations, notably

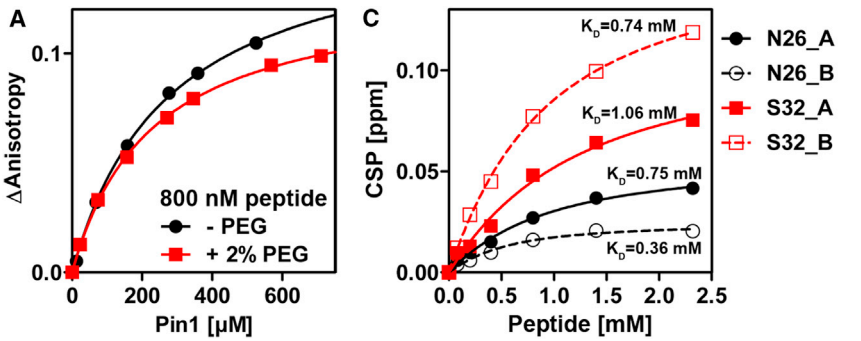

B

	Measured K_D [μM]	Extrapolated K_D from anisotropy [μM]
- PEG400	275 ± 15.2	315
+ 2% PEG400	227 ± 7.3	155

D

	Measured K_D [μM]
Population A	1150 ± 370
Population B	500 ± 150

Figure 5. The Two Conformations of Pin1 Differ in Their Affinity toward Phosphorylated Peptide Ligands

(A) Fluorescence anisotropy titration of 800 nM of Rhodamine B-labeled GGGApSPF peptide by adding increasing amounts of Pin1 protein in the presence (red) and absence (black) of PEG400.

(B) Macroscopic K_D values measured for the fluorescent peptide derived from (A) in the presence and absence of PEG400 were used to extrapolate to K_D values corresponding to 100% conformation A (open) and B (closed), respectively. The presence of PEG400 facilitates stronger domain interaction (population B) and increases peptide binding.

(C) Chemical shift perturbation plotted versus peptide concentration for ^{1}H-^{15}N-HSQC titration of Pin1 with the peptide Suc-ApSPF-pNA. Changes in ppm values are depicted for split resonances of the HN signals of residues N26 and S32 in full-length Pin1 upon the addition of increasing amounts of the peptide.

(D) Affinity constants for the open (population A) and closed (population B) conformation. The measured K_D values represent microscopic affinity constants for peptide binding resolved for the open and closed conformations by NMR. Mean values for all shifting residues are listed here.

lock-and-key (Fischer, 1894), induced fit (Koshland, 1958), and conformational selection or population shift (for review see Csermely et al., 2010). Recently, many studies have investigated the functional dynamics and often found conformational selection to be the best explanation of experimental results (Eisenmesser et al., 2005; James et al., 2003; Lange et al., 2008; Tang et al., 2007).

In contrast to most other experimentally studied proteins, Pin1 poses an extreme case because in its open state, its two domains can be regarded as two completely independent proteins connected by a flexible linker. Our results indicate a transient domain interaction at room temperature. Temperature-dependent studies show that the higher temperature eases breaking of interdomain contacts and escape from the bound state into the open state that is likely to be favored entropically. Recently published experiments demonstrate that the free PPIase domain of Pin1 exhibits a 4.5-fold higher catalytic activity than the full-length two-domain protein (Peng et al., 2009), indicating that the WW domain might play a regulatory role for Pin1's catalytic activity. Our peptide titration experiment (Figure 5B) as well as the observed peak splits indicate that the K_D values measured in NMR titrations and fluorescence anisotropy experiments are dictated by the WW domain binding site. This is in agreement with previous reports (Liu et al., 2010; Verdecia et al., 2000). Stronger substrate binding to the WW domain in the closed state of Pin1 supports the notion of a regulatory WW domain (Smet et al., 2005). Two-domain proteins such as Pin1 tend to be envisioned as two independent domains and a flexible linker, like two pearls on a string. Instead, our results suggest a transient domain interaction that facilitates ligand binding to the WW domain (Figure 6).

Close evaluation of MD, chemical shift (Bayer et al., 2003), and spin-label experimental data indicate that domain interaction does not exclusively happen at the confined interface proposed by the crystal structures of full length Pin1, but occurs at a more blurred and fuzzy interfacial region. As observed in various existing crystal structures of Pin1, we added PEG400, which shifts both domains to a more defined interface and, presumably, locks it to the area observed in the crystal structures. The dynamics of the LAO protein involved in arginine binding might be comparable to our system (Silva et al., 2011). However, we report how a nonsubstrate small molecule (PEG400) selects conformations of the closed state. Although the observed differences in binding affinities are small, they may have observable in vivo effects as demonstrated by Chen and colleagues (Chen et al., 2011). Because we used PEG400 as viable but artificial tool for manipulating the conformational states of our domains, it may be speculated whether in the cellular environment, the role of PEG400 may be taken over by a hydrophobic binding partner like a lipid tethering both domains together, or by a substrate protein containing hydrophobic stretches or lipid anchors; however, the actual binding mechanism of such putative regulatory binding partners could be very different from the one of PEG. Because WW domains in multidomain proteins are very often located next to catalytic domains such as E3 ubiquitin ligases (Wegierski et al., 2006), these cellular binding partners may act as crucial allosteric regulatory factors on these proteins.

WW domain-containing proteins play a pivotal role in the assembly of multiprotein networks (Ingham et al., 2005) and are related to a variety of diseases, such as Alzheimer disease (McLoughlin and Miller, 2008), Huntington chorea (Faber et al., 1998), myopathies (Staub and Rotin, 1996), and inflammatory diseases (Wegierski et al., 2006). Additionally, hundreds of ligands have been identified for these WW domains (Ingham et al., 2005), among those a plethora of cellular proteins, but also many viral targets such as the VP40 (Urata and Yasuda, 2010) and GAG (Heidecker et al., 2007) proteins of Epstein-Barr, Marburg, Ebola, and human T cell leukemia viruses. Our findings that small molecular ligands can be used to control WW domain interaction by modulating the binding affinity and hence the catalytic activity of a whole protein may provide an avenue for therapeutic drug development related to this class of proteins.

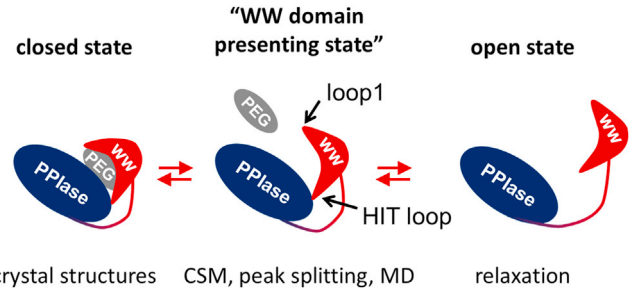

Figure 6. Model for Domain Interaction within Pin1

The Pin1 crystal structures reported in 1997 and 2000 suggested two tightly interacting domains (Ranganathan et al., 1997; Verdecia et al., 2000). Then, NMR relaxation analysis showed little to no domain interaction in solution in the absence of ligands (Bayer et al., 2003; Jacobs et al., 2003). Based on our current data from the interdomain chemical shift mapping (CSM; Figure S3) and the split resonances around the HIT loop of the WW domain, we now postulate an intermediate state that we refer to as WW domain-presenting state, inspired by the upward movement of the WW domain observed in our MD simulations. This intermediate WW domain-presenting state may serve to modulate Pin1-substrate interactions by increasing the affinity toward phosphorylated peptide ligands.

EXPERIMENTAL PROCEDURES

Cloning and Expression of Different Pin1 Constructs

All Pin1 (RefSeq: NM_006221) constructs were cloned into a modified pET-41 vector described elsewhere (Grum et al., 2010) with an N-terminal GST-His_6 fusion protein and a PreScission protease cleavage site.

The triple mutant $Pin1_{S18C/C57A/C113A}$, and $Pin1_{\Delta SSGG}$ with shortened interdomain linker were cloned using the QuikChange Site Directed Mutagenesis kit (Agilent Technologies/Stratagene, Waldbronn, Germany) according to the manufacturer's instructions. Restriction enzymes were purchased from NEB (Frankfurt, Germany) or Fermentas (St. Leon-Rot, Germany); Pfu polymerases were bought from Stratagene (Waldbronn, Germany). All constructs were verified with Sanger sequencing. The amino acid and primer sequences are listed within Tables S2 and S3, respectively.

Thirty milliliter overnight cultures were harvested, resuspended in 1 l lysogeny broth medium, and grown to an optical density 600 (OD_{600}) of 0.8. Subsequently, the cells were pelleted and resuspended in 4 l M9 minimal medium supplemented with 1 g/l [^{15}N]ammonium chloride. After induction of protein expression at OD_{600} = 0.8 with 0.2 mM IPTG, cells were shaken further for 5 hr at 30°C followed by centrifugation. Cell lysis was performed by Microfluidizer (Microfluids, Newton, MA) passages at 4°C in buffer 1 (50 mM potassium phosphate buffer, 1 mM dithiothreitol [DTT], at pH 7.5). The cell lysate was ultracentrifuged, and the supernatant was applied to a Ni-NTA column (GE Healthcare) in buffer 1 supplemented with 20 mM imidazole and then eluted using buffer 1 with 75 mM imidazole; GST-tagged protein was passed over a GSH-sepharose column (GE Healthcare) and eluted in buffer 1 with 10 mM glutathione. His- or GST-tags were cleaved by adding either Thrombin or PreScission protease, respectively. The resulting protein was purified with gel filtration on a Superdex 75PG 16/60 column (GE Healthcare) in 100 mM potassium phosphate buffer, 300 mM KCl, at pH 7.5. Finally, the protein was dialyzed against 50 mM potassium phosphate buffer at pH 6.5 and used directly for NMR spectroscopy.

Paramagnetic Labeling of ^{15}N-$Pin1_{S18C/C57A/C113A}$

The two endogenous cysteine residues Cys57 and Cys113 of human Pin1 were replaced by QuikChange (Stratagene) site-directed mutagenesis and a new cysteine was introduced by changing Ser18 to cysteine. This Pin1 triple mutant, expressed and purified like the wild-type protein described above, was labeled with a paramagnetic PROXYL label as follows: first, 200 μM of $Pin1_{S18C/C57A/C113A}$ were treated with 300 μM TCEP to irreversibly remove disulphide bonds. Next, 3- (2-iodoacetamide)-PROXYL (Sigma Aldrich, Seelze, Germany) dissolved in a 20% ethanol/KP_i at pH 6.5, was added to the protein at a 5-fold molar excess. The sample was then incubated at 4°C overnight. Excessive PROXYL label was removed by washing three times with 50 mM KP_i at pH 6.5 in a Vivaspin concentrator with a molecular weight cutoff of 5,000 Da (Sartorius, Karlsruhe, Germany) at 4°C. Labeling was verified by MALDI-TOF analysis using sinapinic acid in the linear mode: Two masses, 18,586 Da and 18,895 Da, were observed before the labeling reaction, corresponding to the unlabeled protein and a presumed TCEP adduct, respectively. After completion of the reaction, the most prominent peak of 18,785 Da, corresponding to the PROXYL-labeled triple mutant protein, indicated a near quantitative labeling yield (over 80%).

NMR Spectroscopy

NMR experiments were performed on a 600 MHz Unity Inova spectrometer (Varian, Darmstadt, Germany) equipped with a triple resonance probe or on a 700 MHz Ultrashield NMR spectrometer (Bruker, Rheinstetten, Germany) equipped with a cryoprobe (Bruker Biospin). The NMR samples contained 200 μM of ^{15}N-labeled protein, dissolved in 600 μl (H_2O: D_2O/90%: 10%) of 50 mM potassium phosphate buffer at pH 6.5. ^{1}H-^{15}N-SOFAST-heteronuclear multiple quantum correlation (Schanda et al., 2005) and ^{1}H-^{15}N-HSQC experiments were recorded with four scans, 2,048 data points in F2, and 512 data points in F1. Data were processed with the software Topspin 2.1 (Bruker). For apodisation of data, a shifted sine-bell square window function was applied using zero-filling to 4,096 data points in F2 and 2,048 data points in F1 for all spectra.

For the temperature-dependent measurements, ^{1}H-^{15}N-HSQC spectra were recorded in a range from 276 K to 303 K. To correlate peak distance with temperature, only the ^{1}H shifts were regarded. Titration experiments with polyethylene glycol (PEG400; Roth, Karlsruhe, Germany) were performed at 27°C by stepwise addition of 0.2%, 0.6%, 1.0%, 1.7%, and 3.0% of PEG400 to the protein sample. ^{1}H and ^{15}N shifts were combined according to equation G (Ayed et al., 2001):

$$\Delta\delta_{total} = \sqrt{(\Delta\delta_H)^2 + (0.154 \cdot \Delta\delta_N)^2}.$$

Lifetimes were estimated from split signals at 298 K by $\tau = 1/2(\nu_A - \nu_B)$, where ν_A and ν_B are the respective frequencies at maximal height of the signals of states A and B.

Anisotropy Measurements

Fluorescence anisotropy measurements were obtained with a Cary Eclipse fluorescence spectrometer (Varian) equipped with automated polarizer wheels. Fluorescently labeled sample peptide with amidated C terminus (sequence: RhodamineB–GGGApSPF–NH_2) was obtained from ChinaPeptides, Shanghai. Increasing concentrations of Pin1 were added to a fixed concentration of 0.8 μM fluorescent peptide in Tris buffer (20 mM Tris, pH 7.6, 150 mM NaCl, and 3 mM DTT) with and without 2% PEG400 (Roth, Karlsruhe, Germany). After equilibration for 10 min at 20°C, anisotropy was measured in 3 × 3 mm cuvettes (Hellma, Jena, Germany) with excitation wavelength set at 554 nm, emission at 582 nm, and a G-factor of 1.948. Each data point was averaged over 5 min with excitation and emission slits set at 10 nm and 5 nm, respectively. Nonlinear curve fitting was performed in GraphPad Prism 5.04.

K_D values of the open and closed conformation of Pin1 were extrapolated from the K_D values with 2% PEG400 (45% open, 55% closed, K_D = 227 μM) and without PEG400 (75% open, 25% closed, K_D = 275 μM). Therefore, we used the simplified model that the measured peptide binding is an additive result of the binding to the open and closed conformation of Pin1.

Structure Analysis

All structural models evaluated in this study were visualized using YASARA. Model 8 from the NMR ensemble (1NMV) was used as representative structure. The full-length Pin1 structure 2Q5A (Zhang et al., 2007) was complemented with a modeled linker peptide between the WW and PPIase domains both for chemical shift analysis and as a basis for MD simulations. To evaluate a possible binding mode suggested by the *Candida albicans* Ess1 enzyme with a stiff α-helical linker (1YW5; Li et al., 2005), a homology model using the human Pin1 protein sequence based on RefSeq entry NM_006221 was built and also used for chemical shift mapping.

MD Simulations

MD simulations were carried out with GROMACS (Van Der Spoel et al., 2005). Parameters of the PEG400 molecule were obtained with PRODRG (Schüttelkopf and van Aalten, 2004). All MD experiments were carried out using the simulation parameters described in the following. First, structure models were dissolved in water (SPC 216 model) containing neutralizing ions. The overall temperature was kept constant at 300 K with a Nosé-Hoover (Evans and Holian, 1985) thermostat. Lennard-Jones interactions were cut off at 1.0 nm. Electrostatic interactions were modeled with the Particle-Mesh-Ewald method with a cutoff of 1.0 nm and a grid spacing of 0.12 nm. Covalent bond lengths of hydrogen atoms were constrained with the LINCS algorithm (Hess et al., 1997). The G43a1 force field was used. Systems were first energy-minimized with a series of conjugate gradient runs of 500 steps. During the first minimization round, the protein (and PEG400 molecule, if present) were frozen to relax water molecules and ions. In the next minimization, the protein backbone was held fixed while allowing side chain reorientation. In the last minimization, no position restraints were applied. Production simulations ran for a total of 100 ns with 2 fs time steps using the leapfrog algorithm (Van Gunsteren and Berendsen, 2007).

Pareto Optimization

The PPIase domain was taken from X-ray structure 1PIN (Ranganathan et al., 1997) and considered to be fixed. Optimal relative arrangements of PPIase and WW domains were determined in two steps. First, a coarse grid with a spacing of 0.1 nm and 100 grid points along each of the three co-ordinate axes was used to locate promising regions for the paramagnetic label attached to the WW domain. In the second step, these promising regions were refined with a grid of 0.05 nm spacing and again 100 grid points in each of the three directions. Constraints for possible positions were modeled with two optimization functions based on the experimental data. First, we used the experimentally determined extinction radii around the paramagnetic label of 2.09 nm in the presence of PEG, and of 2.25 nm in the absence of PEG. We assumed that for the real position of Cys 18 (standing here for the paramagnetic label), the number of residues inside such an extinction sphere around Cys 18 giving a signal is minimal, as is the number of residues lying outside the sphere and not giving a signal. Ideally, both numbers would be zero. The second optimization function is based on Spearman's rank correlation coefficient ρ of, on one hand, the distance between the paramagnetic label and a residue, and, on the other hand, the extent of extinction of the signal coming from this residue. We assumed that the recovery of the signal monotonously increases with distance. This correlation of distance and recovery of signal should lead to a high ρ for the correct arrangement of the two domains. Technically we subtracted ρ from 1, so that the ideal arrangement leads to $1-\rho = 0$. Pareto dominance in terms of both optimization functions was used to identify arrangements of PPIase and WW domains that best explained the experimental data.

SUPPLEMENTAL INFORMATION

Supplemental Information includes four figures and three tables and can be found with this article online at http://dx.doi.org/10.1016/j.str.2013.07.016.

ACKNOWLEDGMENTS

We cordially thank Peter Binz, Alma Rueppel, and Tina Stratmann for excellent technical assistance. Robert Schwarz is acknowledged for assistance with analyzing HSQC spectra. Thanks to Bettina Warscheid for MS-MALDI measurements of PROXYL-labeled protein preparations.

Received: April 19, 2013
Revised: June 27, 2013
Accepted: July 17, 2013
Published: August 22, 2013

REFERENCES

Arakawa, T., and Timasheff, S.N. (1985). Mechanism of poly(ethylene glycol) interaction with proteins. Biochemistry *24*, 6756–6762.

Ayed, A., Mulder, F.A., Yi, G.S., Lu, Y., Kay, L.E., and Arrowsmith, C.H. (2001). Latent and active p53 are identical in conformation. Nat. Struct. Biol. *8*, 756–760.

Battiste, J.L., and Wagner, G. (2000). Utilization of site-directed spin labeling and high-resolution heteronuclear nuclear magnetic resonance for global fold determination of large proteins with limited nuclear overhauser effect data. Biochemistry *39*, 5355–5365.

Bayer, E., Goettsch, S., Mueller, J.W., Griewel, B., Guiberman, E., Mayr, L.M., and Bayer, P. (2003). Structural analysis of the mitotic regulator hPin1 in solution: insights into domain architecture and substrate binding. J. Biol. Chem. *278*, 26183–26193.

Bayer, E., Thutewohl, M., Christner, C., Tradler, T., Osterkamp, F., Waldmann, H., and Bayer, P. (2005). Identification of hPin1 inhibitors that induce apoptosis in a mammalian Ras transformed cell line. Chem. Commun. (Camb.) (4), 516–518.

Chen, C.H., Martin, V.A., Gorenstein, N.M., Geahlen, R.L., and Post, C.B. (2011). Two closely spaced tyrosines regulate NFAT signaling in B cells via Syk association with Vav. Mol. Cell. Biol. *31*, 2984–2996.

Csermely, P., Palotai, R., and Nussinov, R. (2010). Induced fit, conformational selection and independent dynamic segments: an extended view of binding events. Trends Biochem. Sci. *35*, 539–546.

Duncan, K.E., Dempsey, B.R., Killip, L.E., Adams, J., Bailey, M.L., Lajoie, G.A., Litchfield, D.W., Brandl, C.J., Shaw, G.S., and Shilton, B.H. (2011). Discovery and characterization of a nonphosphorylated cyclic peptide inhibitor of the peptidylprolyl isomerase, Pin1. J. Med. Chem. *54*, 3854–3865.

Eisenmesser, E.Z., Millet, O., Labeikovsky, W., Korzhnev, D.M., Wolf-Watz, M., Bosco, D.A., Skalicky, J.J., Kay, L.E., and Kern, D. (2005). Intrinsic dynamics of an enzyme underlies catalysis. Nature *438*, 117–121.

Evans, D.J., and Holian, B.L. (1985). The Nose-Hoover Thermostat. J. Chem. Phys. *83*, 4069–4074.

Faber, P.W., Barnes, G.T., Srinidhi, J., Chen, J., Gusella, J.F., and MacDonald, M.E. (1998). Huntingtin interacts with a family of WW domain proteins. Hum. Mol. Genet. *7*, 1463–1474.

Fischer, E. (1894). Einfluss der configuration auf die wirkung der enzyme. Ber. Dtsch. Chem. Ges. *27*, 2985–2993.

Gardino, A.K., and Kern, D. (2007). Functional dynamics of response regulators using NMR relaxation techniques. Methods Enzymol. *423*, 149–165.

Gillespie, J.R., and Shortle, D. (1997). Characterization of long-range structure in the denatured state of staphylococcal nuclease. I. Paramagnetic relaxation enhancement by nitroxide spin labels. J. Mol. Biol. *268*, 158–169.

Grum, D., van den Boom, J., Neumann, D., Matena, A., Link, N.M., and Mueller, J.W. (2010). A heterodimer of human 3′-phospho-adenosine-5′-phosphosulphate (PAPS) synthases is a new sulphate activating complex. Biochem. Biophys. Res. Commun. *395*, 420–425.

Guo, C., Hou, X., Dong, L., Dagostino, E., Greasley, S., Ferre, R., Marakovits, J., Johnson, M.C., Matthews, D., Mroczkowski, B., et al. (2009). Structure-based design of novel human Pin1 inhibitors (I). Bioorg. Med. Chem. Lett. *19*, 5613–5616.

Heidecker, G., Lloyd, P.A., Soheilian, F., Nagashima, K., and Derse, D. (2007). The role of WWP1-Gag interaction and Gag ubiquitination in assembly and release of human T-cell leukemia virus type 1. J. Virol. *81*, 9769–9777.

Hess, B., Bekker, H., Berendsen, H.J.C., and Fraaije, J.G.E.M. (1997). LINCS: A linear constraint solver for molecular simulations. J. Comput. Chem. *18*, 1463–1472.

Ingham, R.J., Colwill, K., Howard, C., Dettwiler, S., Lim, C.S., Yu, J., Hersi, K., Raaijmakers, J., Gish, G., Mbamalu, G., et al. (2005). WW domains provide a platform for the assembly of multiprotein networks. Mol. Cell. Biol. *25*, 7092–7106.

Innes, B.T., Bailey, M.L., Brandl, C.J., Shilton, B.H., and Litchfield, D.W. (2013). Non-catalytic participation of the Pin1 peptidyl-prolyl isomerase domain in target binding. Front Physiol *4*, 18.

Jacobs, D.M., Saxena, K., Vogtherr, M., Bernado, P., Pons, M., and Fiebig, K.M. (2003). Peptide binding induces large scale changes in inter-domain mobility in human Pin1. J. Biol. Chem. *278*, 26174–26182.

Jager, M., Deechongkit, S., Koepf, E.K., Nguyen, H., Gao, J., Powers, E.T., Gruebele, M., and Kelly, J.W. (2008). Understanding the mechanism of beta-sheet folding from a chemical and biological perspective. Biopolymers *90*, 751–758.

James, L.C., Roversi, P., and Tawfik, D.S. (2003). Antibody multispecificity mediated by conformational diversity. Science *299*, 1362–1367.

Jaremko, L., Jaremko, M., Elfaki, I., Mueller, J.W., Ejchart, A., Bayer, P., and Zhukov, I. (2011). Structure and dynamics of the first archaeal parvulin reveal a new functionally important loop in parvulin-type prolyl isomerases. J. Biol. Chem. *286*, 6554–6565.

Koshland, D.E. (1958). Application of a Theory of Enzyme Specificity to Protein Synthesis. Proc. Natl. Acad. Sci. USA *44*, 98–104.

Kovermann, M., Zierold, R., Haupt, C., Löw, C., and Balbach, J. (2011). NMR relaxation unravels interdomain crosstalk of the two domain prolyl isomerase and chaperone SlyD. Biochim. Biophys. Acta *1814*, 873–881.

Kühlewein, A., Voll, G., Hernandez Alvarez, B., Kessler, H., Fischer, G., Rahfeld, J.U., and Gemmecker, G. (2004). Solution structure of Escherichia coli Par10: The prototypic member of the Parvulin family of peptidyl-prolyl cis/trans isomerases. Protein Sci. *13*, 2378–2387.

Lange, O.F., Lakomek, N.A., Farès, C., Schröder, G.F., Walter, K.F., Becker, S., Meiler, J., Grubmüller, H., Griesinger, C., and de Groot, B.L. (2008). Recognition dynamics up to microseconds revealed from an RDC-derived ubiquitin ensemble in solution. Science *320*, 1471–1475.

Li, Z., Li, H., Devasahayam, G., Gemmill, T., Chaturvedi, V., Hanes, S.D., and Van Roey, P. (2005). The structure of the Candida albicans Ess1 prolyl isomerase reveals a well-ordered linker that restricts domain mobility. Biochemistry *44*, 6180–6189.

Liou, Y.C., Zhou, X.Z., and Lu, K.P. (2011). Prolyl isomerase Pin1 as a molecular switch to determine the fate of phosphoproteins. Trends Biochem. Sci. *36*, 501–514.

Liu, T., Liu, Y., Kao, H.Y., and Pei, D. (2010). Membrane permeable cyclic peptidyl inhibitors against human Peptidylprolyl Isomerase Pin1. J. Med. Chem. *53*, 2494–2501.

Liu, C., Jin, J., Chen, L., Zhou, J., Chen, X., Fu, D., Song, H., and Xu, B. (2012). Synthesis and biological evaluation of novel human Pin1 inhibitors with benzophenone skeleton. Bioorg. Med. Chem. *20*, 2992–2999.

Lu, K.P., and Zhou, X.Z. (2007). The prolyl isomerase PIN1: a pivotal new twist in phosphorylation signalling and disease. Nat. Rev. Mol. Cell Biol. *8*, 904–916.

Lu, K.P., Hanes, S.D., and Hunter, T. (1996). A human peptidyl-prolyl isomerase essential for regulation of mitosis. Nature *380*, 544–547.

Madl, T., Güttler, T., Görlich, D., and Sattler, M. (2011). Structural analysis of large protein complexes using solvent paramagnetic relaxation enhancements. Angew. Chem. Int. Ed. Engl. *50*, 3993–3997.

McLoughlin, D.M., and Miller, C.C. (2008). The FE65 proteins and Alzheimer's disease. J. Neurosci. Res. *86*, 744–754.

Morcos, F., Chatterjee, S., McClendon, C.L., Brenner, P.R., López-Rendón, R., Zintsmaster, J., Ercsey-Ravasz, M., Sweet, C.R., Jacobson, M.P., Peng, J.W., and Izaguirre, J.A. (2010). Modeling conformational ensembles of slow functional motions in Pin1-WW. PLoS Comput. Biol. *6*, e1001015.

Mueller, J.W., and Bayer, P. (2008). Small family with key contacts: par14 and par17 parvulin proteins, relatives of pin1, now emerge in biomedical research. Perspect. Medicin. Chem. *2*, 11–20.

Mueller, J.W., Link, N.M., Matena, A., Hoppstock, L., Rüppel, A., Bayer, P., and Blankenfeldt, W. (2011). Crystallographic proof for an extended hydrogen-bonding network in small prolyl isomerases. J. Am. Chem. Soc. *133*, 20096–20099.

Namanja, A.T., Peng, T., Zintsmaster, J.S., Elson, A.C., Shakour, M.G., and Peng, J.W. (2007). Substrate recognition reduces side-chain flexibility for conserved hydrophobic residues in human Pin1. Structure *15*, 313–327.

Namanja, A.T., Wang, X.J., Xu, B., Mercedes-Camacho, A.Y., Wilson, K.A., Etzkorn, F.A., and Peng, J.W. (2011). Stereospecific gating of functional motions in Pin1. Proc. Natl. Acad. Sci. USA *108*, 12289–12294.

Peng, J.W., Wilson, B.D., and Namanja, A.T. (2009). Mapping the dynamics of ligand reorganization via 13CH3 and 13CH2 relaxation dispersion at natural abundance. J. Biomol. NMR *45*, 171–183.

Ranganathan, R., Lu, K.P., Hunter, T., and Noel, J.P. (1997). Structural and functional analysis of the mitotic rotamase Pin1 suggests substrate recognition is phosphorylation dependent. Cell *89*, 875–886.

Schanda, P., Kupce, E., and Brutscher, B. (2005). SOFAST-HMQC experiments for recording two-dimensional heteronuclear correlation spectra of proteins within a few seconds. J. Biomol. NMR *33*, 199–211.

Schüttelkopf, A.W., and van Aalten, D.M. (2004). PRODRG: a tool for high-throughput crystallography of protein-ligand complexes. Acta Crystallogr. D Biol. Crystallogr. *60*, 1355–1363.

Sekerina, E., Rahfeld, J.U., Müller, J., Fanghänel, J., Rascher, C., Fischer, G., and Bayer, P. (2000). NMR solution structure of hPar14 reveals similarity to the peptidyl prolyl cis/trans isomerase domain of the mitotic regulator hPin1 but indicates a different functionality of the protein. J. Mol. Biol. *301*, 1003–1017.

Silva, D.A., Bowman, G.R., Sosa-Peinado, A., and Huang, X. (2011). A role for both conformational selection and induced fit in ligand binding by the LAO protein. PLoS Comput. Biol. *7*, e1002054.

Smet, C., Wieruszeski, J.M., Buée, L., Landrieu, I., and Lippens, G. (2005). Regulation of Pin1 peptidyl-prolyl cis/trans isomerase activity by its WW binding module on a multi-phosphorylated peptide of Tau protein. FEBS Lett. *579*, 4159–4164.

Staub, O., and Rotin, D. (1996). WW domains. Structure *4*, 495–499.

Tang, C., Schwieters, C.D., and Clore, G.M. (2007). Open-to-closed transition in apo maltose-binding protein observed by paramagnetic NMR. Nature *449*, 1078–1082.

Urata, S., and Yasuda, J. (2010). Regulation of Marburg virus (MARV) budding by Nedd4.1: a different WW domain of Nedd4.1 is critical for binding to MARV and Ebola virus VP40. J. Gen. Virol. *91*, 228–234.

Van Der Spoel, D., Lindahl, E., Hess, B., Groenhof, G., Mark, A.E., and Berendsen, H.J. (2005). GROMACS: fast, flexible, and free. J. Comput. Chem. *26*, 1701–1718.

Van Gunsteren, W.F., and Berendsen, H.J.C. (2007). A Leap-frog Algorithm for Stochastic Dynamics. Mol. Simul. *1*, 173–185.

Verdecia, M.A., Bowman, M.E., Lu, K.P., Hunter, T., and Noel, J.P. (2000). Structural basis for phosphoserine-proline recognition by group IV WW domains. Nat. Struct. Biol. *7*, 639–643.

Wegierski, T., Hill, K., Schaefer, M., and Walz, G. (2006). The HECT ubiquitin ligase AIP4 regulates the cell surface expression of select TRP channels. EMBO J. *25*, 5659–5669.

Xu, G.G., Slebodnick, C., and Etzkorn, F.A. (2012). Cyclohexyl ketone inhibitors of Pin1 dock in a trans-diaxial cyclohexane conformation. PLoS ONE *7*, e44226.

Yeh, E.S., and Means, A.R. (2007). PIN1, the cell cycle and cancer. Nat. Rev. Cancer *7*, 381–388.

Zhang, Y., Daum, S., Wildemann, D., Zhou, X.Z., Verdecia, M.A., Bowman, M.E., Lücke, C., Hunter, T., Lu, K.P., Fischer, G., and Noel, J.P. (2007). Structural basis for high-affinity peptide inhibition of human Pin1. ACS Chem. Biol. *2*, 320–328.